공학석사 학위논문

Design and Synthesis of Conjugated Copolymer Based on Rearranged Pechmann Dye for Polymer Solar Cells

고분자 태양 전지를 위한

재배열된 페크만 염료 기반 공액 고분자의

설계 및 합성

2014년 2월

서울대학교 대학원

재료공학부

서 상 덕

Abstract

Design and Synthesis of Conjugated Copolymer Based on Rearranged Pechmann Dye for Efficient Polymer Solar Cells

Suh, Sang Duk

Department of Materials Science and Engineering

Seoul National University

D-A type alternating conjugated copolymers (PRPD3T, PRPDBDT-O, PRPDBDT-T) were synthesized by using a new electron acceptor unit rearranged Pechmann dye (RPD) with thiophene, 4,8-bis(2-ethyl-hexyloxy) benzo[1,2-b;4,5-b']dithiophene, and 4,8-bis(2-(2-ethyl-hexylthienyl) benzo [1,2-b;4,5-b']dithiophene as electron donor units. The copolymers have wide band gap and exhibit high open circuit voltage. Furthermore, conjugated random copolymer PRPDDPP composed of RPD and diketopyrrolopyrrole (DPP) as co-electron acceptor unit was synthesized. Complementary absorption rage of RPD and DPP makes PRPDDPP absorb light from 300 nm to 900 nm. Consequently, PRPDDPP exhibits a PCE of 2.40% an open circuit voltage of 0.75 V, a short circuit current density of 5.55 $mAcm^{-2}$, and a fill factor of 0.58 under AM 1.5G condition.

Keywords: Rearranged Pechmann dye, polymer solar cells, wide bandgap polymer, random copolymer

Student Number: 2012-20605

Contents

List of Schemes

List of Figures

List of Tables

1. Introduction

At present, most of the world energy consumes originates from fossil fuels. However, along with the diminishing of reserve volume of fossil fuels and environmental problems caused by the use of fossil fuels, the need toward the development of renewable energy sources has become urgent in recent years. One potential alternative to fossil fuels is utilizing solar cells which can directly convert solar energy into electricity.[1] Today, inorganic solar cells based on multi-layer single crystalline silicon have achieved power conversion efficiencies of up to 40%.[2] Nevertheless, the high cost of silicon-based solar cells limited their widespread and large-scale usage. Polymer solar cells (PSCs) have been regarded as one of the most promising candidates for alternatives of silicon-based solar cells because of the possibility of a production on flexible and large-area substrates by solution processing which should dramatically reduce the manufacturing costs.[3-5]

A fundamental difference between PSCs and inorganic solar cells is that light absorption results in the formation of excitons in organic semiconducting materials, rather than in free electrons and holes. Exciton is coulombicly bound electron hole pair and the coulombic binding energy is approximately 0.3 eV. To separate the generated exciton into free charge carriers, exciton should diffuse to donor/acceptor interface. At the interface, the energy offset between the donor and acceptor LUMO energy level is utilized to dissociate excitons.[6-9] To succeed this process, device structure and energy level of donor and acceptor materials are very important. The most widely utilized device

structure of PSCs is bulk heterojunction (BHJ), where a nanoscale phase separated blend of donor and acceptor was sandwiched between a transparent electrode and a metal electrode. Optimized BHJ structure has large degree of interlayer contact between donor and acceptor, which helps exciton reach to D/A interface within its diffusion length. [5, 10]

From a point of material view, the development of donor materials plays a more critical role on the recent progresses of BHJ-PSCs due to the choice of acceptor materials is limited.[11-13] Especially, the energy levels of donor materials have a big impact on the performances of PSCs. At first, the LUMO energy levels of polymer donors have to be at least 0.3 eV higher than those of PCBM to separate exciton. Additionally, the energy level difference between the HOMO of the polymer donor and the LUMO of the acceptor is correlated with V_{OC}.[14] In theory, polymers with low-lying HOMO levels would exhibit higher V_{OC}. However, the HOMO level of the polymer donor cannot go too low. This is because continuously lowering the HOMO level of the polymer donor would inevitably enlarge the band gap of the polymer, diminishing the light absorbing ability of the polymer donor (thereby a low J_{SC}). Therefore, energy level tuning is the most important factor when designing polymer donor.

Donor-acceptor (D-A) type copolymer is now widely utilized as polymer donor because of its possibility of effective energy level tuning.[15-17] In the D-A type copolymer main backbone, electron donating units (donor unit) and electron withdrawing units (acceptor unit) are located alternatively. D-A type concept was first proposed by Havinga *et al*. in 1992.[18] The principle of the

D-A concept is based on the internal charge transfer (ICT) from a donor unit to an acceptor unit as known as push-pull effect.[19] The hybridization of the D-A structure leads to a broadening of the valence and conduction bands and thus results in bandgap reduction by raising the HOMO level and lowering the LUMO level in conjugated polymer. In such D–A copolymer systems, the HOMO level is mainly affected by the donor unit, and the LUMO level is mainly affected by the acceptor unit. Thus both HOMO and LUMO energy levels can be easily tuned by choosing different donor and acceptor units.[20-23]

The electron acceptor unit is required to contain electron withdrawing group in its structure. To withdraw electron, atoms which have higher electronegativity than carbon such as nitrogen, oxygen and fluorine have to be used. They are utilized as a form of imine (–C=N-) or carbonyl group (-C=O) to diminish the donating effect of their lone pair electrons. [24]

Rearranged Pechmann dye (RPD) can be a promising candidate of new electron acceptor unit. Its chemical structure is similar to diketopyrrolopyrrole (DPP); the only difference is that it contains naphthyridine instead of pyrrolopyrrole. Because the core of RPD is symmetric naphyridine and contains two carbonyl groups, it is electron-deficient, planar and fully conjugated like DPP. Furthermore, its solubility can be effectively controlled by various aryl- or alkyl-amines, which affects solid-state packing and morphology. [25]

The first Pechmann dye (PD) was unwittingly synthesized in 1882 by Hans von Pechmann in an attempt to prepare 1,4-naphthoquinone from β-benzoyl acrylic acid.[26] And PD is known to isomerize under basic conditions

and/or at elevated temperatues in alcoholic solvents to yield its corresponding 6,6'-dilactone counterparts, known as rearranged Pechmann dye.[27] These were benzene based material, and thiophene based PD and RPD were first synthesized by *Sullvian* et al. in 2011 and studied their optoelectric properties.[24,28]

In this study, rearranged Pechmann dye (RPD) was synthesized and polymerized with basic electron donor units to apply to PSCs. As counterparts of RPD, we selected thiophene and benzodithiophene (BDT). Thiophene is the most basic electron donor unit and BDT was recently reported to have excellent charge transport ability due to its symmetric and planar structure and have a suitable balance between bandgap and HOMO.[29,30] Furthermore, to increase J_{SC} by extending light absorption, RPD was polymerized with DPP as a random copolymer because of its complementary light absorption range to RPD.[31] Accordingly, we synthesized four conjugated copolymers of PRPD3T, PRPDBDT-O, PRPDBDT-T and PRPDDPP. RPD is utilized as the electron acceptor unit in all four polymers, and especially used as co-electron acceptor unit with DPP in PRPDDPP. Thiophene, 4,8-bis(2-ethyl-hexyloxy) benzo[1,2-b;4,5-b']dithiophene and 4,8-bis(2-(2-ethyl-hexylthienyl) benzo[1,2-b;4,5-b']dithiophene is used as the electron donor units in each polymers. The optical, electrochemical and charge transport properties of polymers as well as photovoltaic performance of the PSCs are extensively examined in terms of molecular energy levels. Also morphological study of the polymer/PCBM blend was performed to understand the performance of the PSC device based on RPD-based conjugated polymers.

2. Experimental Section

2.1 Materials

All reagents were purchased from Sigma-Aldrich unless otherwise specified and used as received. Dichloromethane, toluene and Dimethyl formide (DMF) was purchased from Samjun Chemicals and freshly purified by solvent purifier (PS-Micro, Innovative technology). [6,6]-phenyl-C_{71}-butyric acid methyl ester ($PC_{71}BM$) was obtained from Nano-C and poly(3,4-ethylenedioxythiophene):poly(styrene sulfonate) (PEDOT:PSS) (Baytron P VP AI 4083) was purchased from H.C. Stark and passed through a 0.45 μm PVDF syringe filter before spin-coating.

2.2. Synthesis of monomer

2.2.1. Synthesis of 2-hexyl-decyl bromide (1)

A solution of PPh_3 (50 g, 0.191 mol) in CH_2Cl_2 (300 mL) was purged with argon for 15 minutes at 0 °C, which was followed by addition of Br_2 (30.52 g, 9.77 mL, 0.191 mol) at RT. 2-Hexyl-decanol (46.31 g, 0.191 mmol) was added dropwise via additional funnel over 0.5 h and the reaction solution was stirred at RT. for 12 h. After removal of CH_2Cl_2 the residue was washed with hexane and filtered. The filtrate was concentrated via rotary evaporation and the resulting crude yellow oil was purified via column chromatography (hexane:CH_2Cl_2=4:1). The title compound **1** was isolated as colorless oil (53.07, 91% yield). ^{1}H NMR (300 MHz, $CDCl_3$) δ (ppm): 3.46 (d, J = 6.0 Hz,

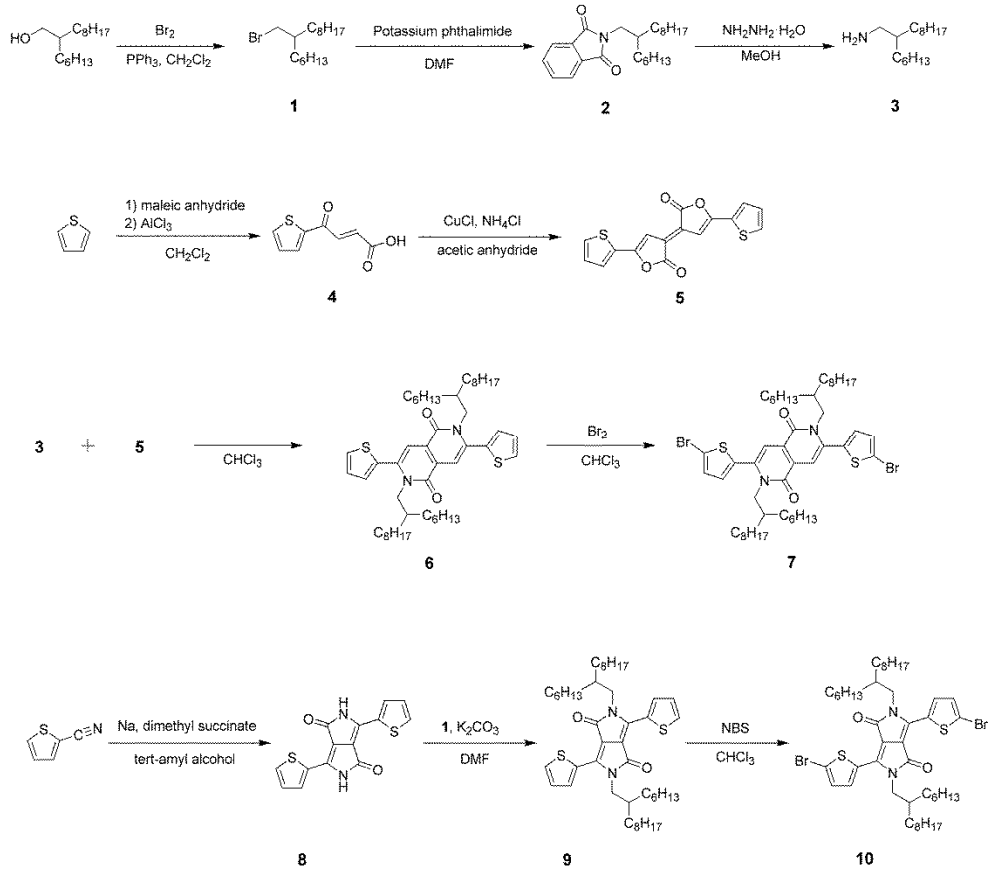

Scheme 2.1 The whole synthetic route of monomers

2H), 1.59 (m, 1H), 1.35 (m, 24H), 0.91 (m, 6H).

2.2.2. Synthesis of *N*-(2-hexyl-decyl)phthalimide (2)

Potassium phthalimide (7.41 g, 0.04 mol) was added to a solution of 2-hexyldecylbromide **1** (11.48 g, 0.0376 mol) in DMF (45 mL). The reaction was stirred at 90°C for 18 h. After cooling to r.t., the reaction mixture was poured into H_2O (200 mL) and extracted with CH_2Cl_2 (3 × 100 mL). The combined organic layer was washed with 0.2 N KOH (200 mL), H_2O (200 mL), and saturated NH_4Cl (200 mL), dried over anhydrous $MgSO_4$, and concentrated under reduced pressure after filtration. The resulting crude yellow oil was purified via column chromatography to afford **2** as a colorless oil (13.41 g, 96% yield). ^{1}H NMR (300 MHz, $CDCl_3$) δ (ppm): 7.85 (m, 2H), 7.72 (m, 2H), 3.57 (d, J = 9.0 Hz, 2H), 1.88 (m, 1H), 1.28 (m, 24H), 0.86 (m, 6H).

2.2.3. Synthesis of 2-hexyl-decylamine (3)

N-(2-hexyl-decyl)phthalimide **2** (7.80 g, 0.021 mol), hydrazine hydrate (hydrazine, 51 %) (4mL, 0.065 mol) and MeOH (100 mL) were stirred at 95ºC and monitored by TLC. After disappearance of the starting imide, MeOH was removed under reduced pressure and the residue was diluted with CH_2Cl_2 (200 mL) and washed with 10% KOH (2 × 100 mL). The combined aqueous layer was extracted with CH_2Cl_2 (3 × 50 mL). The combined organic layer was washed with brine (2 × 100 mL) and dried over $MgSO_4$. After removal of CH_2Cl_2, the product **3** was obtained as yellow oil (4.26 g, 84%

yield), which can be used without further purification. ^{1}H NMR (300 MHz, $CDCl_3$) δ (ppm): 2.60 (d, J = 5.0 Hz, 2H), 1.39 (m, 1H), 1.26 (br, 24H), 0.88 (m, 6H).

2.2.4. Synthesis of (E)-4-oxo-4-(thien-2-yl)but-2-enoic acid (4)

Thiophene (5 g, 0.059 mol) and maleic anhydride (6.41 g, 0.065 mol) were dissolved with stirring in CH_2Cl_2 (200 mL) submerged in an ice bath. $AlCl_3$ (15.85 g, 0.119 mol) was added portion-wise and the mixture turned from colorless to orange to dark brown. The mixture was stirred in the ice bath for 30 minutes and then allowed to stir at RT for 16 h. The mixture was poured into ice cold 1M HCl (100 mL) and stirred for 2 h. The organic layer was separated and the washed with water, brine and dried over magnesium sulfate. After concentration, the residue was suspended in hexane and filtered affording **4** as a light orange solid which was recrystallized from EtOAc. (5.4 g, 49.9 %). ^{1}H NMR (300 MHz, DMSO-d6) δ (ppm): 8.16 (d, 1H), 8.05 (d, 1H), 7.86 (d, 1H), 7.32 (dd, 1H), 6.82 (d, 1H)

2.2.5. Synthesis of (E)-5,5'-(thien-2-yl)-2H,2'H-[3,3'-bifuranylidene]-2,2'-dione (5)

A 50 mL round-bottomed flask was charged with **4** (3 g, 0.016 mol), CuCl (0.60 g, 0.006 mol), NH_4Cl (0.65 g, 0.012 mol) and acetic anhydride (25 mL). The mixture was brought to reflux with stirring whereupon the mixture turned dark purple. After 2h, the mixture was cooled and the solid collected by vacuum filtration and washed with acetic acid, ethanol and ether successively.

The dark solid was dissolved in chloroform and subjected to flash chromatography (chloroform) to afford **5** as light blue crystals (0.7 g, 40%). ^{1}H NMR ($CDCl_3$, 300MHz) δ (ppm): 7.64 (d, 2H), 7.60 (d, 2H), 7.35 (s, 2H), 7.20 (dd, 2H).

2.2.6. Synthesis of 2,6-bis-(2-hexyl-decyl)-3,7-di(thien-2-yl)-2,6-naphthyridine-1,5(2H,6H)-dione (6)

Pechmann dye **5** (1.2 g, 0.0036 mol) and 2-hexyl-decylamine (3.53 g, 0.015 mol) were dissolved in chloroform (20 mL) and stirred over 18 h. To the clear orange solution formed, $TsOH \cdot H_2O$ (4.18 g, 0.022 mol) was added, causing the mixture to turn green-blue immediately. After 3h, water was added and the two layers transferred into a separatory funnel (chloroform) and separated. The organic layer was washed with 1M HCl, saturated $NaHCO_3$ solution, dried over sodium sulfate and evaporated to dryness. The residue was subjected to flash chromatography (CH_2Cl_2/n-hexane 3:7) to afford **6** (1.12 g, 19 %). ^{1}H NMR ($CDCl_3$, 300MHz) δ(ppm): 7.45 (d, 2H), 7.17 (d, 2H), 7.11 (t, 2H), 7.10 (s, 2H), 4.27 (m, 4H), 1.63 (m, 2H), 1.04-1.17 (m, 48H), 0.67-0.81 (m, 12H).

2.2.7. Synthesis of 3,7-bis-(5-bromo-thien-2-yl)-2,6-bis-(2-hexyl-decyl)-2,6-naphthyridine-1,5(2H,6H)-dione (7)

Rearranged Pechmann dye **6** (0.5 g, 0.0013 mol) was dissolved with stirring in chloroform (20 mL). Br_2 (0.43 g, 0.0027 mol) was added dropwise and the solution was stirred at RT over 12h. After sodium thiosulfate 1M solution (10 mL) was added and the solution was stirred 2h. Two layers transferred into a

separatory funnel and separated. The organic layer was washed with brine, saturated $NaHCO_3$ solution, dried over sodium sulfate and evaporated to dryness. The residue was subjected to flash chromatography (toluene:n-hexane=1:1) to afford **7** (0.48 g, 68.5 %). ^1H NMR ($CDCl_3$, 300MHz) δ(ppm): 7.06 (d, 2H), 7.05 (s, 2H), 6.93 (d, 2H), 4.17 (d, 4H), 1.70 (s, 2H), 1.09-1.21 (m, 48H), 0.82-0.89 (m, 12H).

2.2.8. Synthesis of 3,6-di(thien-2-yl)pyrrolo[3,4-c]pyrrole-1,4(2H, 5H)-dione (8)

A 500 mL three-neck flask connected to a condenser was charged with a stir bar and tert-amyl alcohol (250 mL). Sodium metal (2.56 g, 108 mmol) immersed in mineral oil was thoroughly washed with hexanes and cut into small pieces. The sodium metal pieces were slowly added to the reaction mixture over a 1.5 h period while the temperature was slowly increased to 120 °C over the same amount of time. After all the sodium metal pieces were dissolved, thiophene-2-corbonitrile (11.9 g, 108 mmol) was added to the reaction. As dimethyl succinate (5.29 g, 36.2 mmol) was added dropwise to the reaction mixture over 1 h, the solution turned dark red. The reaction contents were stirred at 120 °C for 2 h, and then precipitated into acidic MeOH (400 mL MeOH and 20 mL conc. HCl). Filtration of the suspension through a Buchner funnel yielded **8** as a dark red solid (9.10 g, 83%). ^1H NMR ($CDCl_3$, 300MHz) δ(ppm): 7.06 (d, 2H), 7.05 (s, 2H), 6.93 (d, 2H), 4.17 (d, 4H), 1.70 (s, 2H), 1.09-1.21 (m, 48H), 0.82-0.89 (m, 12H).

2.2.9. Synthesis of 2,5-bis(2-hexyl-decyl)-3,6-di(thien-2-yl)pyrrolo [3,4-c]pyrrole-1,4(2H,5H)-dione (9)

In a dry three-neck 250 mL round bottom flask was charged with **8** (7.0 g, 23.3 mmol), and K_2CO_3 (9.0 g, 69.9 mmol) were dissolved in dry DMF (250 mL). and heated to 120 °C under argon for 1 h. And then 2-lhexyl-decylbromide (17.74 g, 58.3 mmol) was added drop-wise, and the reaction mixture was further stirred and heated overnight at 130 °C. The reaction mixture was allowed to cool down to RT, poured into water, and stirred for 30min. The product was extracted with chloroform, then washed with water, and dried over magnesium sulfate. Removal of the solvent afforded the crude product which was further purified using column chromatography on silica gel using a mixture of hexane and chloroform as eluent, giving the product as a purple solid. (11.0g, 53.5%). ^{1}H NMR ($CDCl_3$, 300MHz) δ(ppm): 8.89 (d, 2 H), 7.61 (d, 2 H), 7.25 (at, 1 H), 4.01 (m, 4 H), 1.92 – 1.78 (m, 2 H), 1.40 – 1.18 (m, 16 H), 0.89 – 0.83 (t, 8.8 Hz, 12 H).

2.2.10. Synthesis of 3,6-bis(5-bromothien-2-yl)-2,5-bis(2-hexyl-decyl)pyrrolo[3,4-c]pyrrole-1,4(2H,5H)-dione (10)

N-bromosuccininide (1.26g, 7.08 mmol) was added slowly to a solution of the compound **9** (3g, 3.08mmol) in $CHCl_3$ (100mL). The solution was protected from light and stirred at room temperature for 48 h. The reaction mixture was poured into water (100 mL) and extracted with CHCl3. The organic layer was dried over magnesium sulfate and the solvent was evaporated under reduced pressure. Purification by flash chromatography (20 % hexanes in $CHCl_3$)

yielded a purple solid (1.7g, 52 %). ^{1}H NMR ($CDCl_3$, 300MHz) δ(ppm): 8.64 (d, 2 H), 7.22 (d, 2 H), 3.92 (m, 4 H), 1.88 – 1.78 (m, 2 H), 1.39 – 1.19 (m, 16 H), 0.90 – 0.84 (t, 12 H).

2.3. Synthesis of polymers

2.3.1. Synthesis of poly(thiophene)-*alt*-(3,7-bis-(thiophen-2-yl)-2,6-bis-(2-hexyl-decyl)-2,6-naphthyridine-1,5(2H,6H)-dione), (PRPD3T)

After 160.4 mg of the compound **7** (0.17 mmol) and 71.0 mg (0.17 mmol) of 2,5-bis(trimethylstannyl)thiophene was dissolved in dry toluene (4 ml) and dry DMF (0.4ml) in a reaction vial under nitrogen, the solution was degassed for 30min, and then 6.1 mg of tetrakis(triphenylphosphine)palladium(0) (5.3 μmol) was quickly added to the solution. The mixture was degassed for an additional 10minutes after which the vial is sealed and stirred for 5 hours at 150℃ in a microwave reactor, followed by end-capping using 2-bromothiophene and 2-(tributylstannyl)thiophene for 15min respectively. After cooling down to room temperature, the solution was precipitated in methanol. And the precipitates were filtered onto the Soxhlet thimble, and then purified by Soxhlet extraction by methanol, acetone, hexane and then chloroform. Finally the chloroform fraction was concentrated, and the precipitated again in methanol. The PRPD3T was obtained as a orange solid which was obtained after filtering by PTFE filter and dried overnight. Yield: 97.6 mg (85.3%)

2.3.2. Synthesis of poly(4,8-bis(2-ethyl-hexyloxy)benzo[1,2-b;4,5-b']dithiophene)-*alt*-(3,7-bis-(thiophen-2-yl)-2,6-bis-(2-hexyl-decyl)-2,6-naphthyridine-1,5(2H,6H)-dione), (PRPDBDT-O)

After 144 mg of the compound **7** (0.15 mmol) and 120 mg (0.15 mmol) of 2,6-bis(trimethylstannyl)-4,8-bis(2-ethyl-hexyloxy)benzo[1,2-b;4,5-b'] dithiophene was dissolved in dry toluene (4 ml) and dry DMF (0.4ml) in a reaction vial under nitrogen, the solution was degassed for 30min, and then 6.1 mg of tetrakis(triphenylphosphine)palladium(0) (5.3 μmol) was quickly added to the solution. The mixture was degassed for an additional 10minutes after which the vial is sealed and stirred for 5 hours at 150℃ in a microwave reactor, followed by end-capping using 2-bromothiophene and 2-(tributylstannyl)thiophene for 15min respectively. After cooling down to room temperature, the solution was precipitated in methanol. And the precipitates were filtered onto the Soxhlet thimble, and then purified by Soxhlet extraction by methanol, acetone, hexane and then chloroform. Finally the chloroform fraction was concentrated, and the precipitated again in methanol. The PRPD3T was obtained as a orange solid which was obtained after filtering by PTFE filter and dried overnight. Yield: 173.0 mg (82.5%)

2.3.3. Synthesis of poly(4,8-bis(2-ethyl-hexylthienyl)benzo[1,2-b;4,5-b']dithiophene)-*alt*-(3,7-bis-(thiophen-2-yl)-2,6-bis-(2-hexyl-decyl)-2,6-naphthyridine-1,5(2H,6H)-dione), (PRPDBDT-T)

PRPDBDT-T was prepared through same procedure of preparation of PRPDBDT-O except using 2,6-bis(trimethylstannyl)-4,8-bis(2-ethyl-hexylthienyl) benzo[1,2-b;4,5-b']dithiophene instead of 2,6-

bis(trimethylstannyl)-4,8-bis(2-ethyl-hexyloxy)benzo[1,2-b;4,5-b'] dithiophene in the polymerization step. Yield: 185.0 mg (87.5%)

2.3.4. Synthesis of poly(([2,2']bithiophenyl-5-yl-2,5-bis-(2-hexyl-decyl)-6-thiophen-2-yl-2,5-dihydro-pyrrolo[3,4-c]pyrrole-1,4-dione)-*co*-(3,7-bis-(thiophen-2-yl)-2,6-bis-(2-hexyl-decyl)-2,6-naphthyridine-1,5(2H,6H)-dione), (PRPDDPP)

After compound **7** (120mg, 0.13 mmol), compound **10** (116mg, 0.13 mmol) and 106 mg (0.26 mmol) of 2,5-bis(trimethylstannyl)thiophene was dissolved in dry toluene (5 ml) and dry DMF (0.5ml) in a reaction vial under nitrogen, the solution was degassed for 30 min, and then 8.7 mg of tetrakis(triphenylphosphine)palladium(0) (7.6 μmol) was quickly added to the solution. The mixture was degassed for an additional 10minutes after which the vial is sealed and stirred for 5 hours at 150℃ in a microwave reactor, followed by end-capping using 2-bromothiophene and 2-(tributylstannyl)thiophene for 15min respectively. After cooling down to room temperature, the solution was precipitated in methanol. And the precipitates were filtered onto the Soxhlet thimble, and then purified by Soxhlet extraction by methanol, acetone, hexane and then chloroform. Finally the chloroform fraction was concentrated, and the precipitated again in methanol. The PRPD3T was obtained as a dark green solid which was obtained after filtering by PTFE filter and dried overnight. Yield: 172.3 mg (71.3%)

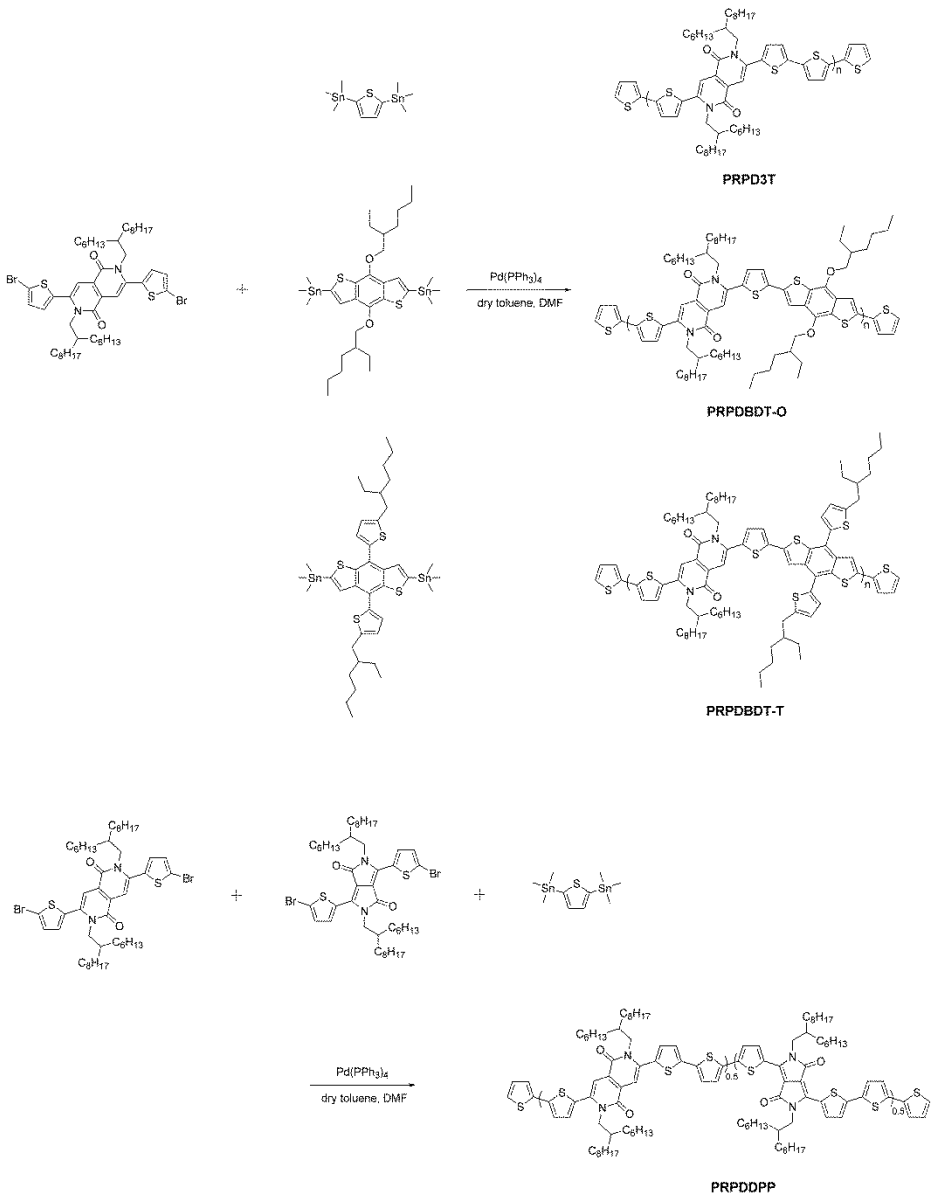

Scheme 2.2 The synthetic scheme polymers

2.4. Characterization

The chemical structures of materials used in this study were identified by ^{1}H NMR spectra obtained from a Brucker Avance DPX 300 NMR spectrometer with deuterted chloroform, DMSO acetone as solvents. Molecular weight and its distribution were measured by gel permeation chromatography (Waters) equipped with a Waters 2414 refractive index detector using $CHCl_3$ as an eluent, where the columns were calibrated against standard polystyrene samples. The optical absorption spectra wre obtained by UV-Vis spectrophotometer (Lambda 25, Perkin Elmer). Cyclic voltammetery experiments were carried out on potentiostat/galvanostat (VMP 3, Biologic) in an electrolyte solution of 0.1 M tetrabutylammonium hexafluorophosphate (Bu_4NPF_6) in acetonitrile. Three-electrode cell was used for all cylic voltammetry experiments. Platinum wires and gold rod were used as counter and working electrods, respectively, and silver/silver ion (Ag in 0.1M $AgNO_3$ solution, Bioanalytical System Inc.) was used as a reference electrode. X-Ray Diffraction patterns were recorded with New D8 Advance diffractometer using Cu Kα (λ=0.154 nm) radiation. The thin film morphology was characterized by transmission electron microscopy (TEM) with a JEOL JEM1010 operating in 80 kV of acceleration voltage. For TEM measurement, the solar cell device was immersed in deionized water and then the active layer was floated onto the Cu grid.

2.5. Device fabrication and measurements

2.5.1. Materials

ITO-patterned glass was used as an anode in PSC device. The sheet resistance of the ITO was less than 10 Ω/square. $PC_{71}BM$ were obtained from Nano-C and used as received. PEDOT:PSS (Clevios P VP AI 4083) was purchased from H.C. Stark and passed through a 0.45 μm PVDF syringe filter before spin-coating.

2.5.2. Solar cell device fabrication

Polymer solar cells were fabricated on ITO glass cleaned by stepwise sonication in acetone and IPA, followed by O_3 plasma treatment for 10 min. PEDOT:PSS was spin-coated on the ITO glass at 4000 rpm for 30 s and annealed at 150℃ for 30 min to yield 40 nm thick film. A mixture of polymer and $PC_{71}BM$ was dissolved in anhydrous solvent and spin-coated on the top of the ITO/PEDOT:PSS film. The typical thickness of the active layer was 80-110 nm. Calcium (20 nm) and aluminum (100 nm) were evaporated under vacuum lower than 10^{-6} Torr on the top of active layer through a shadow mask. The effective area of cell was ca. 4 mm^2

2.5.3. Solar cell performance measurements

The photovoltaic performance was measured under nitrogen atmosphere inside the glove box. The current-voltage (*J-V*) curves of the device were obtained on a computer-controlled Keithley 4200 source measurement unit under AM 1.5G (100 mW/cm^2) simulated by an Oriel solar simulator (Oriel

91160A). The light intensity was calibrated using a NREL-certified photodiode prior to each measurement. The external quantum efficiency (EQE) was measured using Polaronix K3100 IPCE measurement system (McScience). The light intensity at each wavelength was calibrated with a standard single-crystal Si cell.

2.5.4. Device fabrication for hole mobility measurement by SCLC.

Devices were fabricated on ITO glass cleaned by stepwise sonication in acetone and IPA, followed by O_3 plasma treatment for 10 min. PEDOT:PSS was spin-coated on the ITO glass at 4000 rpm for 30 s and annealed at 150℃ for 30 min to yield 40 nm thick film. A mixture of polymer and $PC_{71}BM$ was dissolved in anhydrous solvent and spin-coated on the top of the ITO/PEDOT:PSS film. The typical thickness of the active layer was 80-110 nm. Gold was evaporated under vacuum lower than 10^{-6} Torr on the top of active layer through a shadow mask. The effective area of cell was ca. 4 mm^2

3. Results and Discussion

3.1. Synthesis and Characterization

The chemical structures of of 2-hexyl-decyl bromide (**1**), *N*-(2-hexyl-decyl)phthalimide (**2**), 2-hexyl-decylamine (**3**), (E)-4-oxo-4-(thien-2-yl)-but-2-enoic (**4**), (E)-5,5'-(thien-2-yl)-2H,2'H-[3,3'-bifuranylidene]-2,2'-dione (**5**), 2,6-bis-(2-hexyl-decyl)-3,7-di(thien-2-yl)-2,6-naphthyridine-1,5(2H,6H)-dione (**6**), 3,7-bis-(5-bromo-thien-2-yl)-2,6-bis-(2-hexyl-decyl)-2,6-naphthyridine-1,5(2H,6H)-dione (**7**), 3,6-di(thien-2-yl)pyrrolo[3,4-c]pyrrole-1,4(2H, 5H)-dione (**8**), 2,5-bis(2-hexyl-decyl)-3,6-di(thien-2-yl)pyrrolo [3,4-c]pyrrole-1,4(2H,5H)-dione (**9**), Synthesis of 3,6-bis(5-bromothien-2-yl)-2,5-bis(2-hexyl-decyl)pyrrolo[3,4-c]pyrrole-1,4(2H,5H)-dione (**10**), PRPD3 T, PRPDBDT-O, PRPDBDT-T and PRPDDPP are identified by ^{1}H NMR, as shown in Figure 3.1–10, respectively. The molecular weight and polydispersity index as measured by gel permeation chromatography are listed in Table 3.1.

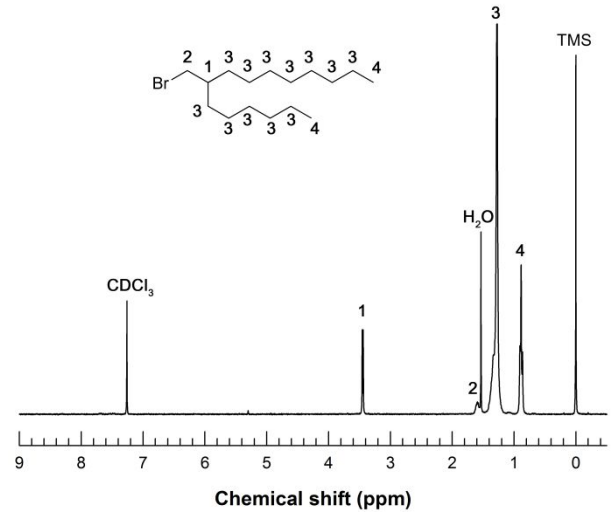

Figure 3.1 Chemical structure and ^{1}H NMR spectrum of 2-hexyl-decyl bromide

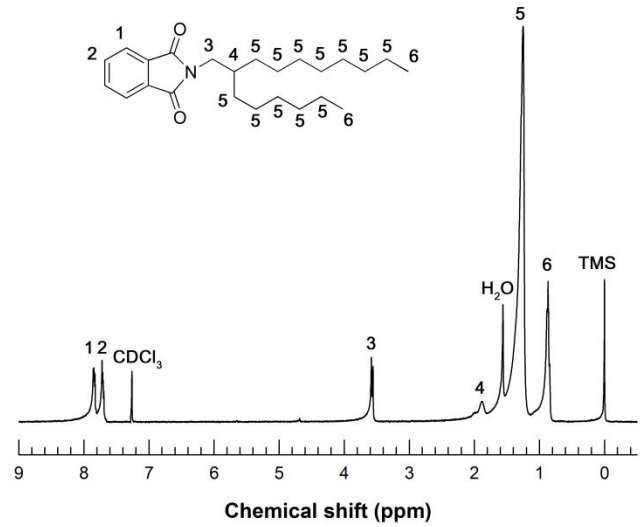

Figure 3.2 Chemical structure and ^{1}H NMR spectrum of of *N*-(2-hexyl-decyl)phthalimide

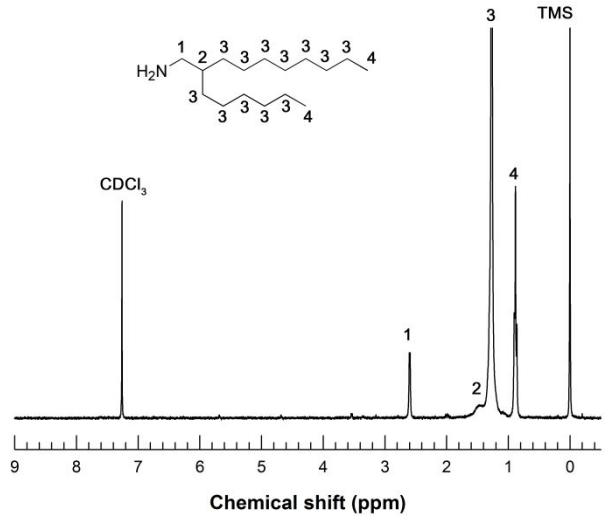

Figure 3.3 Chemical structure and ^{1}H NMR spectrum of 2-hexyl-decylamine

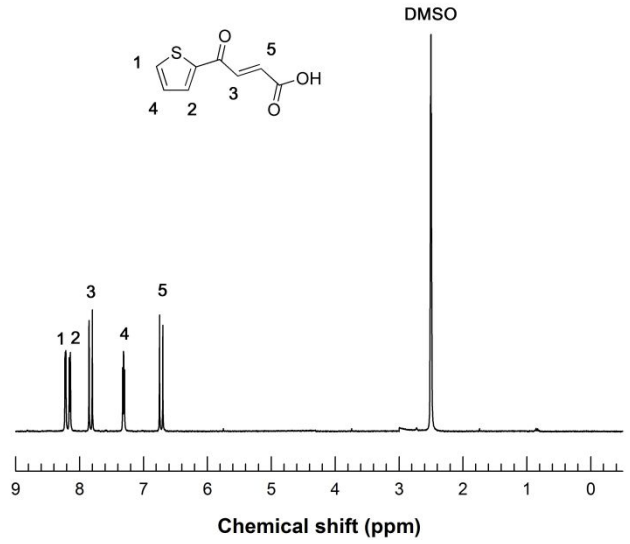

Figure 3.4 Chemical structure and ^{1}H NMR spectrum of (E)-4-oxo-4-(thien-2-yl)-but-2-enoic acid

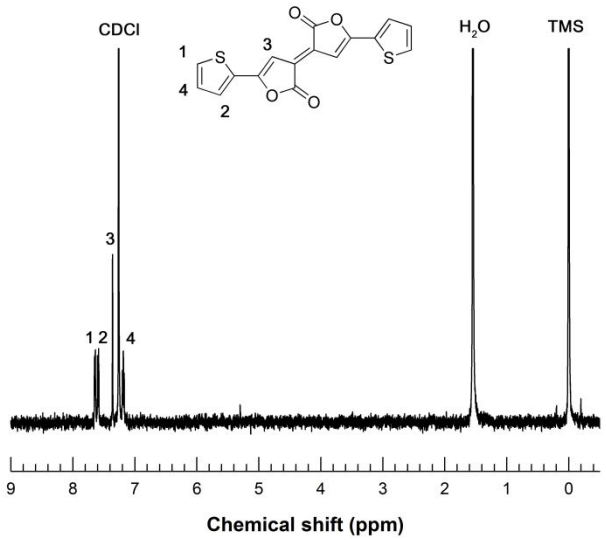

Figure 3.5 Chemical structure and ^{1}H NMR spectrum of of (E)-5,5'-(thien-2-yl)-2H,2'H-[3,3'-bifuranylidene]-2,2'-dione

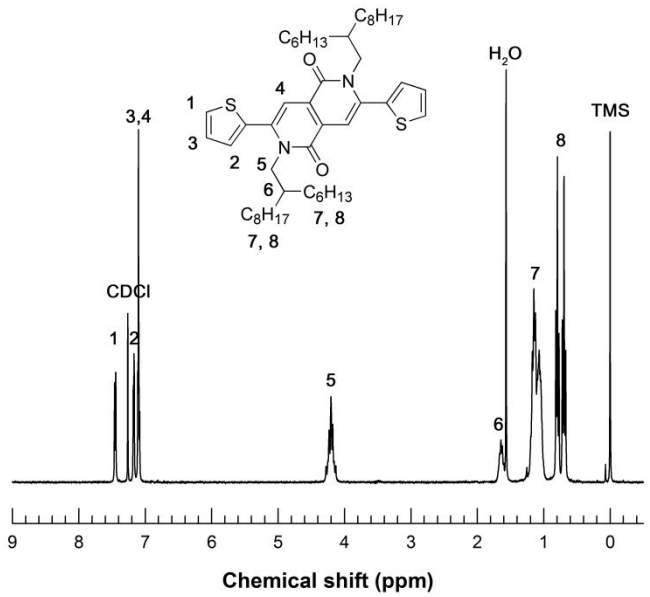

Figure 3.6 Chemical structure and ^{1}H NMR spectrum of 2,6-bis-(2-hexyl-decyl)-3,7-di(thien-2-yl)-2,6-naphthyridine-1,5(2H,6H)-dione

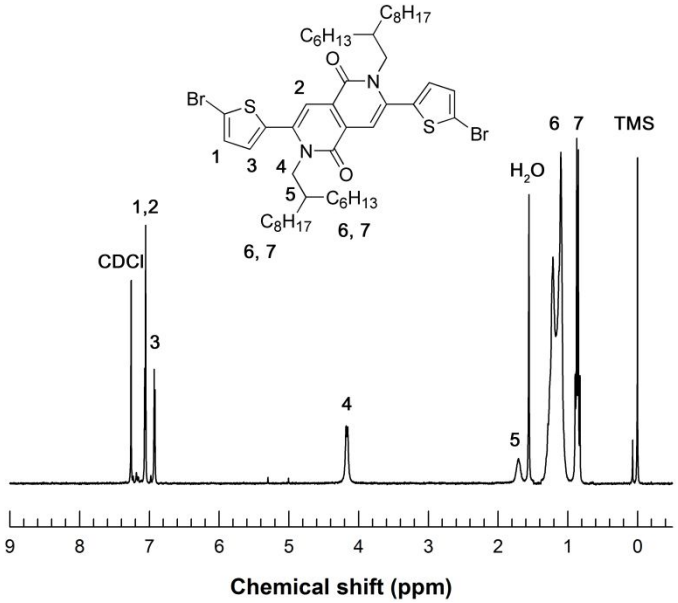

Figure 3.7 Chemical structure and ^{1}H NMR spectrum of 3,7-bis-(5-bromo-thien-2-yl)-2,6-bis-(2-hexyl-decyl)-2,6-naphthyridine-1,5(2H,6H)-dione

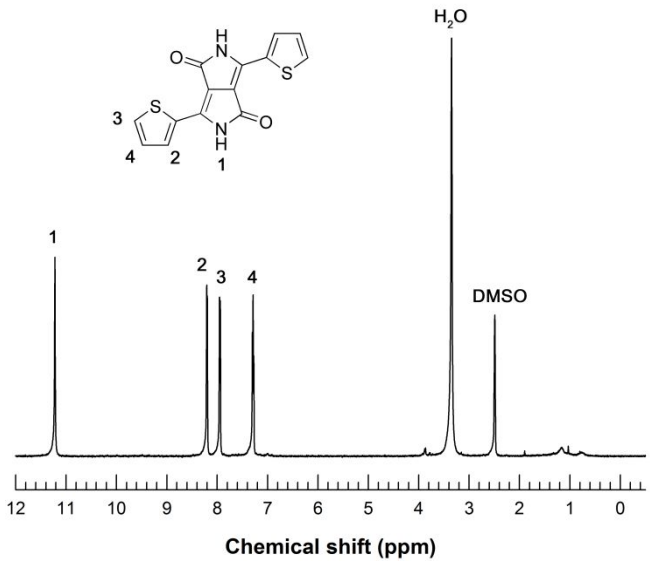

Figure 3.9 Chemical structure and ^{1}H NMR spectrum of of 3,6-di(thien-2-yl)pyrrolo[3,4-c]pyrrole-1,4(2H, 5H)-dione

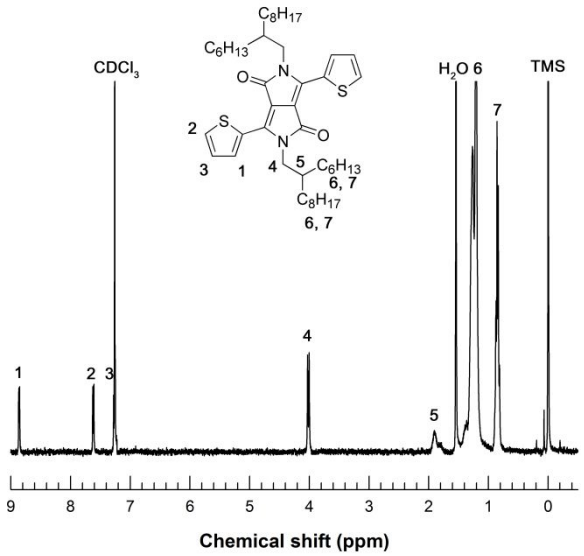

Figure 3.9 Chemical structure and ^{1}H NMR spectrum of of 2,5-bis(2-hexyl-decyl)-3,6-di(thien-2-yl)pyrrolo [3,4-c]pyrrole-1,4(2H,5H)-dione

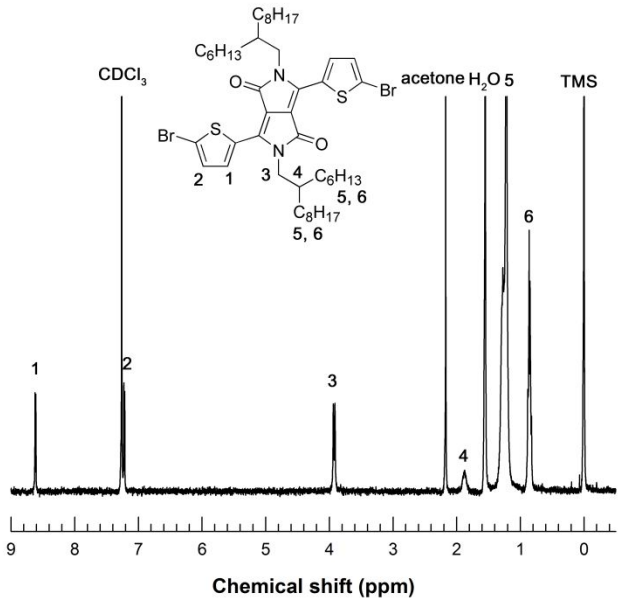

Figure 3.10 Chemical structure and ^{1}H NMR spectrum of 2,5-bis(2-hexyl-decyl)-3,6-di(thien-2-yl)pyrrolo [3,4-c]pyrrole-1,4(2H,5H)-dione

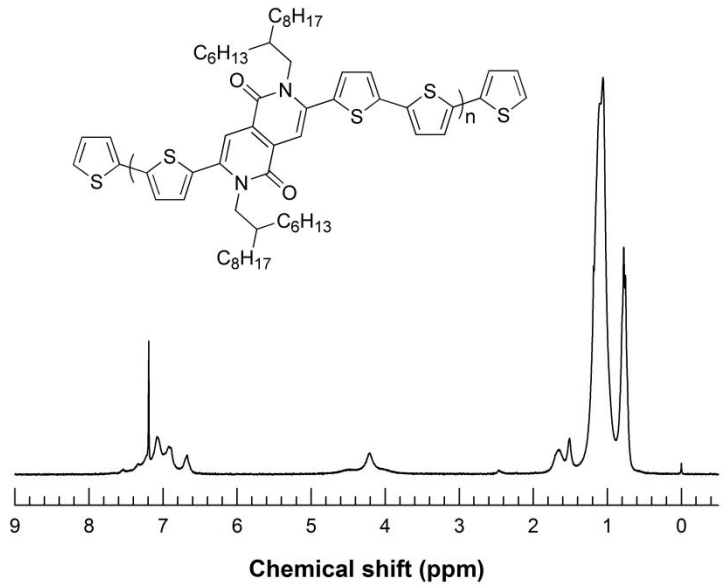

Figure 3.11 Chemical structure and ^{1}H NMR spectrum of PRPD3T

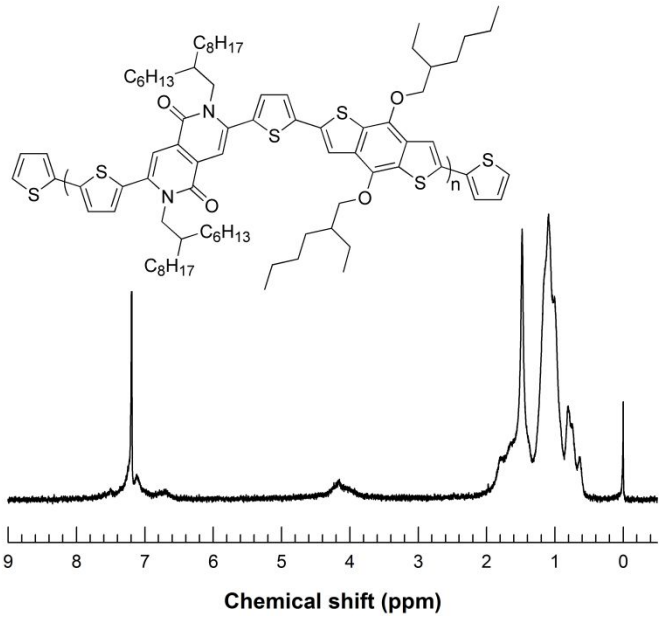

Figure 3.12 Chemical structure and ^{1}H NMR spectrum of PRPDBDT-O

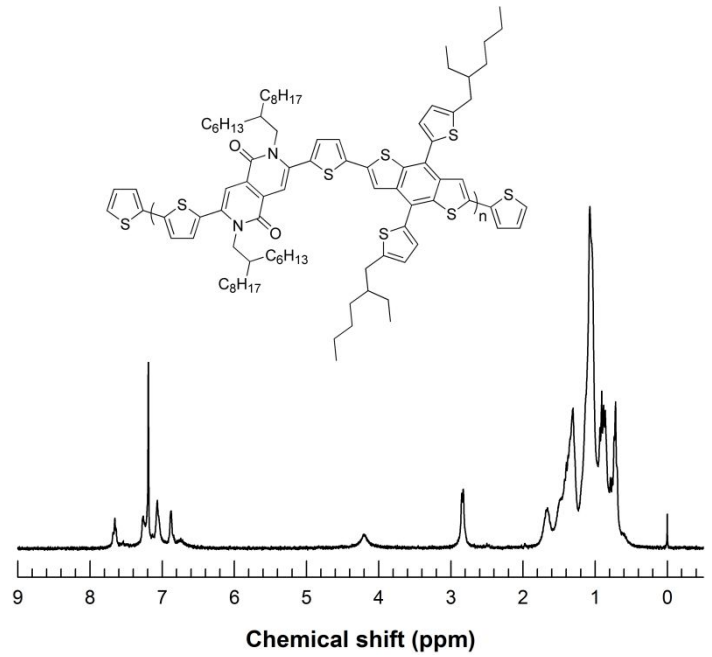

Figure 3.13 Chemical structure and ^{1}H NMR spectrum of PRPDBDT-T

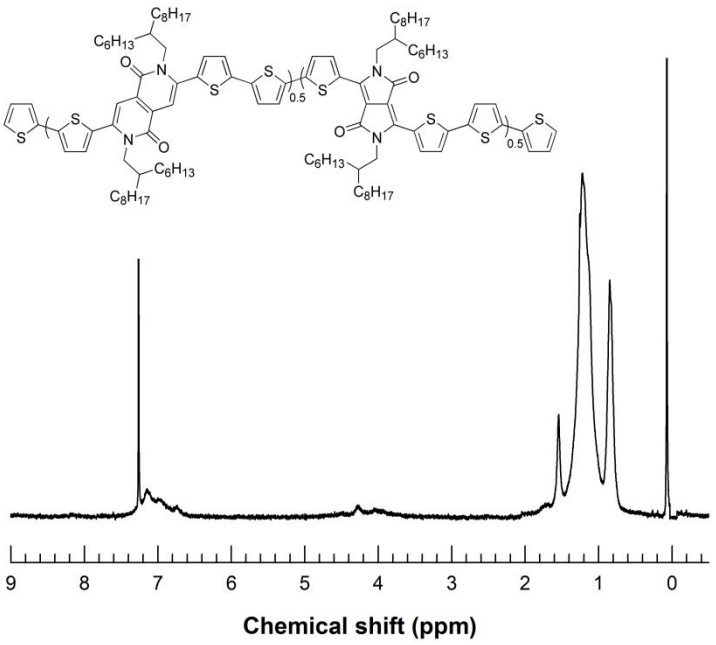

Figure 3.14 Chemical structure and ^{1}H NMR spectrum of PRPDDPP

3.2. Optical properties

The optical properties of the polymers were investigated by ultraviolet-visible (UV-Vis) absorption spectroscopy. Fig 3.15 shows the absorption spectrum of PRPD3T, PRPDBDT-O, PRPDBDT-T and PRPDDPP in dilute chloroform solution and as spin-coated films on glass substrate. As shown in Fig. 3.15, the three polymers PRPD3T, PRPDBDT-O and PRPDBDT-T showed similar absorption maximums (λ_{max}) at 454 nm, 479 nm, and 466 nm, with a full-width-at-half- maximum (FWHM) of 106 nm, 118 nm, and 113 nm in solution, respectively. As compared to them, PRPDDPP shows two distinguishable absorption peaks. The first peak of which the absorption maximum is at 453 nm with FWHM of 132 nm results from the absorption of RPD unit, and the second peak of which the absorption maximum is 714 nm at with FWHM of 192 nm results from the absorption of DPP unit. Because DPP units substitute for the half of RPD units, extinction coefficient of the first peak is about half of that of the other three polymers. Moreover, DPP unit has wider absorption range and higher extinction coefficient than RPD unit, which results in large absorption of photons at long wavelength range.

After spin-coated into the thin film, λ_{max} of PRPD3T, PRPDBDT-O and PRPDBDT-T located at 458 nm, 485 nm, and 469 nm, respectively. They are red-shifted about 4 nm, 6 nm, and 3 nm from their solution absorption peak, indicating that the polymeric backbones form π–π stacks in the solid state.[32] The FWHM of PRPD3T, PRPDBDT-A, and PRPDBDT-T in the film was 115 nm, 138 nm, and 153 nm, respectively. Compared to PRPD3T and PRPDBDT-O, the enhanced FWHM of PRPDBDT-T can be readily ascribed

to regular alkyl chain and enlarged conjugation of 2D-BDT.[33] This broader absorption of PRPDBDT-T in film indicates its slightly stronger light-harvesting ability, which is an important factor affecting the current density of PSCs. In case of PRPDDPP, λ_{max} of the first and second peak located at 465 nm and 728 nm, respectively with a red-shift of 12 nm and 14 nm compared to their solution absorption peak and FWHM of PRPDDPP in each peak is 157, 232nm. These data and vibronic shoulder peak shown in long wavelength range mean PRPDDPP form π–π stacks well in the solid state. [34]

Optical bandgaps (E_g^{opt}) calculated from the film absorption edge (λ_{edge}) of PRPD3T, PRPDBDT-O, PRPDBDT-T and PRPDDPP are 2.29 eV, 2.21 eV, 2.23 eV and 1.40 eV, respectively. From the bandgaps, RPD based polymers can be regarded as wide bandgap polymer compared to the reported D-A polymers. And as we can see in the absorption spectra of PRPDDPP, when RPD is combined with low bandgap material, it can complement the absorption of short wavelength range which low bandgap material doesn't absorb. Consequently, the extending absorption range makes PSCs utilize sun light more efficiently.

3.3. Electrochemical properties

The electrochemical data of the polymer is obtained from the oxidation and reduction cyclic voltamograms, as shown in Fig. 3.9, and summarized in Table 3.2. The HOMO energy level of the polymer was calculated using the equation: HOMO = $-[E_{ox} - E_{1/2}(\text{ferrocene}) + 4.8]$ V, where $E_{1/2}$(ferrocene) and E_{ox} is the onset oxidation potential of ferrocene and polymer vs. Ag/Ag^+

respectively. The LUMO energy level was also estimated by using the equation: LUMO = – [E_{red} – $E_{1/2}$(ferrocene) + 4.8] V, where E_{red} is the onset reduction potential of the polymer.

As shown in Table 3.2, the HOMO and LUMO energy levels of the polymers are determined to be –5.58 and –3.53 eV for PRPD3T, –5.52 and –3.35 eV for PRPDBDT-O, –5.51 and –3.41 eV for PRPDBDT-T, and –5.36 and –3.96 eV for PRPDDPP, respectively. Generally, LUMO energy levels measured by cyclic voltammetry are known to be inaccurate.[35] To obtain accurate LUMO energy levels, LUMO energy levels were recalculated from the HOMO energy levels and optical bandgap by using equation: LUMO = HOMO + E_g^{opt}. Recalculated LUMO energy levels for PRPD3T, PRPDBDT-O, PRPDBDT-T and PRPDDPP are –3.29, –3.45, –3.43 eV and –3.96 eV, respectively. From these high-lying LUMO energy levels, RPD unit can be regarded as weak electron acceptor units.

PRPDBDT-O and PRPDBDT-T show similar HOMO and LUMO energy levels, indicating that alkyl chains on the BDT unit hardly affect the energy levels of the polymers. On the other hand, the strong donating ability of thiophene compared to BDT derivatives makes the HOMO energy level of PRPD3T lie slightly higher than BDT based polymers. Since the open circuit voltage (V_{OC}) of polymer is linearly dependent on the difference between the HOMO energy level of the electron donor and the LUMO energy level of the electron acceptor, the deep HOMO energy level of the donor polymer is expected to afford high V_{OC} for the resulting polymer solar cells. Accordingly, we can expect BDT based polymers to have high V_{OC} resulting from their

deep HOMO energy levels.

PRPDDPP shows the highest-lying HOMO energy level and lowest-lying LUMO energy level among the four polymers. This is because DPP unit has higher-lying HOMO energy level and lower-lying LUMO energy level than RPD unit. When orbital hybridization occurs in the D-A type polymer, LUMO energy level of polymer is determined by LUMO energy levels of its building blocks. The lower LUMO energy level lies, the more it influences on the LUMO energy level of the polymer. Likewise, the higher HOMO energy level lies, the more it influences on the HOMO energy level of the polymer. Therefore, RPD unit is not the determining factor of energy level but DPP in case of PRPDDPP. The difference of HOMO and LUMO energy level between PRPD3T and PRPDDPP is 0.22 eV and 0.67 eV, which means the effect of DPP is larger on LUMO energy level than HOMO energy level. Because HOMO energy level of polymer is mainly determined by thiophene.

3.4. Structural properties

X-ray diffraction (XRD) patterns of PRPD3T, PRPDBDT-O, PRPDBDT-T, PRPDDPP, PRPD3T/$PC_{71}BM$, PRPDBDT-O/$PC_{71}BM$, PRPDBDT-T/$PC_{71}BM$ and PRPDDPP/$PC_{71}BM$ were investigated as shown in Fig. 3.10. The samples were prepared by drop-casting on the silicon wafer.

Diffraction peaks at near 5º are (100) peaks which are ascribed to the interchain distance separated by the alkyl side chains, while weak peaks at near 25º are (100) peaks which can be assigned to the π–π stacking between polymeric backbones.[36] Each sample shows (100) peaks and from these peaks,

the corresponding interchain distances are derived by using the Bragg formula of $2d\sin\theta = \lambda$, herein $\lambda = 0.154$ nm. Interchain distances of each sample are determined to be 18.3 Å for PRPD3T, 14.8 Å for PRPDBDT-A, 18.2 Å for PRPDBDT-T, 18.7 Å for PRPDDPP, 17.8 Å for PRP3T/ $PC_{71}BM$, 14.6 Å for PRPDBDT-O/$PC_{71}BM$, 17.1 Å for PRPDBDT-T/$PC_{71}BM$ and 18.3 Å for PRPDDPP/$PC_{71}BM$. PRPD3T and PRPDDPP show not only (100) peaks but also (200) and (300) peaks, which implies a highly organized assembly of these π-conjugated polymers at solid state. Among the pristine films, PRPDBDT-O shows the shortest interchain distance, at the same time, solely displays (010) peaks.

After blending with $PC_{71}BM$, the intensity of (100) peaks and interchain distance of the polymers decreased. Especially, (200) and (300) peak of PRPD3T and PRPDDPP and (010) peak of PRPDBDT-T disappear. This can be explained by the interruption of polymer network from $PC_{71}BM$. All the blended films show relatively strong diffraction peaks appearing around 2θ = 15-23º which is mainly ascribed to the short-range order of $PC_{71}BM$ (2θ = 19.2º, d = 4.6 Å). In case of PRPDBDT-T, this peak is not sharp compared to the other polymers. These differences can be explained by the effect of alkylthienyl group. When BDT is substituted to 2-hexyl-decylthienyl chain, the intermolecular interaction is weakened due to the weakly polarized thiophene compared to oxygen and the distortion between the thiophene and BDT units. This weakens aggregation ability of PRPDBDT-T, resulted in better miscibility with $PC_{71}BM$.[37] This can also explain that intensity of (100) peak of PRPDBDT-T decreases much larger than that of other polymers.

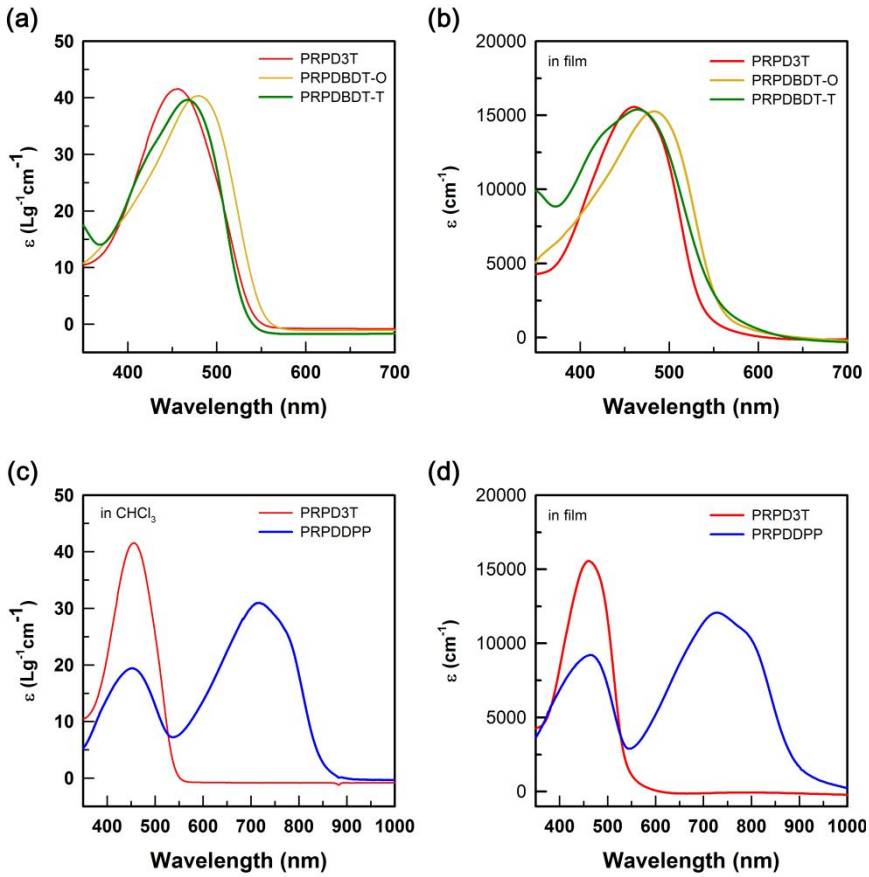

Figure 3.15 UV-Vis absorption spectrum of the polymers in $CHCl_3$ solution (a), (c) and in film (b), (d).

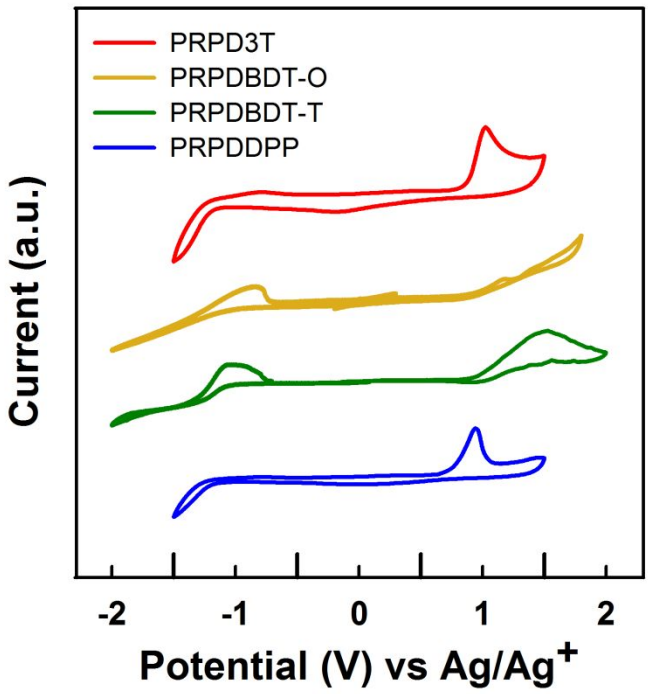

Figure 3.16 Cyclic voltammogram of the polymers

Table 3.1 Summary of properties of the polymers

Polymer	M_n (kDa)	PDI	λ_{max} (nm)/FWHM (nm)		$E_g^{opt[a]}$ (eV)	E_{HOMO} (eV)	$E_{LUMO}^{[b]}$ (eV)	$E_{LUMO}^{[c]}$ (eV)
			Solution	Film				
PRPD3T	22.0	1.79	454/106	458/115	2.29	–5.58	–3.53	–3.29
PRPDBDT-O	34.3	1.38	479/118	485/138	2.21	–5.66	–3.71	–3.45
PRPDBDT-T	25.7	1.34	466/113	469/153	2.23	–5.67	–3.65	–3.44
PRPDDPP	24.2	2.06	453,714/ 132,192	465,728 / 157,232	1.40	–5.36	–3.71	–3.96

[a] is optical bandgap in film

[b] is measured by cyclic voltammetry.

[c] is calculated from the HOMO level and the optical bandgap. LUMO = HOMO + E_g^{opt}

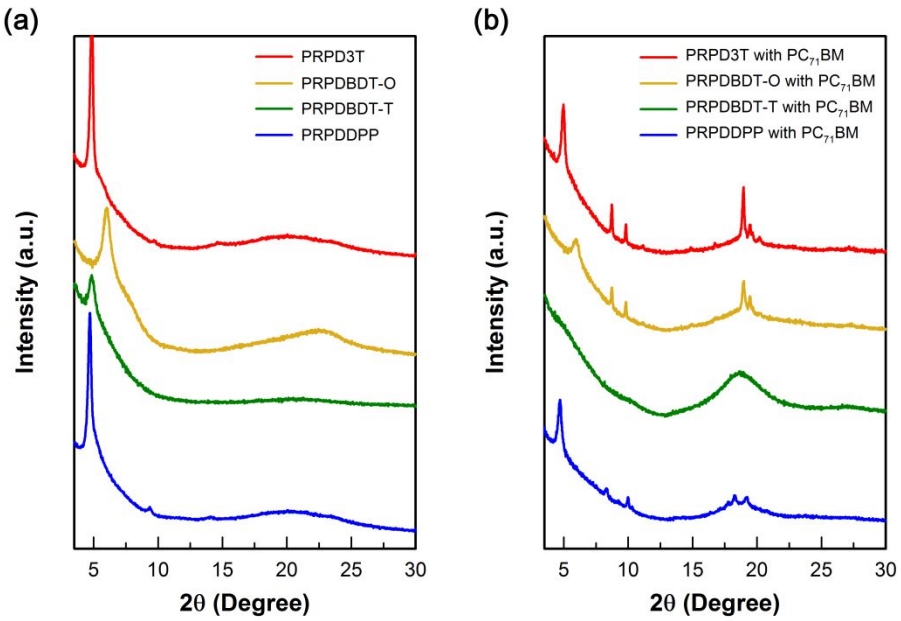

Figure 3.17 X-ray diffraction (XRD) patterns of the polymers and blend with $PC_{71}BM$

3.5. Photovoltaic properties

The polymer solar cells were fabricated with a layered configuration of glass/ITO/PEDOT:PSS/polymer:$PC_{71}BM$/Ca/Al. The *J*–*V* characteristics of photovoltaic devices prepared from polymer:$PC_{71}BM$ using various solvents and additive are represented in Figure 3.11, and their photovoltaic parameters are summarized in Table 3.3. Optimized blend ratio of polymer:$PC_{71}BM$ was 1:2 in all polymers.

The V_{OC} of PRPD3T based device is 0.86 V, which is slightly lower than that of PRPDBDT-O and PRPDBDT-T which is 0.91 V and 0.92 V, respectively. Since V_{OC} is linearly dependent on the difference between the HOMO energy level of polymer and the LUMO energy level of the $PC_{71}BM$, the deep HOMO energy level of BDT based polymers show higher V_{OC} for the resulting PSCs than PRPD3T. The J_{SC} is shown as 2.48 $mAcm^{-2}$ for PRPD3T, 2.82 $mAcm^{-2}$ for PRPDBDT-O and 3.55 $mAcm^{-2}$ for PRPDBDT-T. Though PRPDBDT-T has similar extinction coefficient to PRPD3T and PRPDBDT-O, FWHM of PRPDBDT-T is larger than that of other two polymers because of enlarged conjugation of 2D-BDT. This broader absorption of PRPDBDT-T in film means its slightly stronger light-harvesting ability, resulting in high J_{SC}. The fill factor (FF) of PRPD3T, PRPDBDT-O and PRPDBDT-T is 0.30, 0.29 and 0.43, respectively. High FF of PRPDBDT-T implies that high J_{SC} of it is not only contribution of broader absorption. Consequently, PRPDBDT-T based PSC shows 1.39 % of PCE which is higher than 0.64% of PRPD3T and 0.75% of PRPDBDT-O.

When DPP units substitute for the half of RPD units, PRPDDPP shows a

V_{OC} = 0.75 V, J_{SC} = 5.55 mA cm^{-2}, FF = 0.58, and PCE = 2.40%. Though its V_{OC} diminishes to 0.75 V due to its high-lying HOMO energy level, its J_{SC} and FF is much higher than the other three polymers. The extending of absorption edge from about 550 nm to 900 nm by DPP units with high extinction coefficient make polymer absorb much more light because roughly 70% of the sunlight energy is distributed in the wavelength region from 380 to 900 nm.[38] Consequently, the increasing light harvesting ability results in formation of more excitons and high J_{SC} of PRPDDPP based PSCs.

The external quantum efficiency (EQE) of the devices under monochromatic light is shown in Fig 3.19. EQE and absorption spectrum (Fig 3.15) exhibits similar tendency. PRPD3T, PRPDBDT-O and PRPDBDT-T generate photocurrent in the range of 300–700 nm. The photocurrent generated in the range from 550 to 700nm is responsible for $PC_{71}BM$. In case of PRPDDPP, generated photocurrent difference between short wavelength rage and long wavelength range is not large in spite of its extinction coefficient difference. That means internal quantum efficiency (IQE) of RPD unit is better than DPP unit.

3.6. Charge transport characteristics

To investigate the charge carrier transport characteristics, we measured the hole mobility of polymer/$PC_{71}BM$ blend films from the space charge limited current (SCLC) hole mobility measurement. The SCLC hole mobilities can be measured by the standard methods. The single-carrier mobility can be extracted from the dark current density-voltage (J_D-V) curve and is caclulated

by the trap-free space charge limited current model at low reverse applied voltage using the Mott-Gurney square law: $J = (9/8)\varepsilon_0\varepsilon_r\mu(V^2/L^3)$, where ε_0 is vacuum permittivity, ε_r is dielectric constant of the transport material (assumed 3 for all polymers), μ is drift mobility of each charge carrier, V is effective applied voltage, and L is the thickness of the polymer film. Then, the mobility is obtained from the slope of plot of $J_{1/2}$ vs V_a-V_{bi} (Fig 3. 20), where V_a is the applied potential and V_{bi} is the built-in potential which results from the difference in the work function of the anode and the cathode. The devices were fabricated with a layered configuration of glass/ITO/PEDOT:PSS/ polymer:$PC_{71}BM$/Au. The active layers were spin-coated under the conditions that afford the best photovoltaic results, and Au was deposited 40 nm. Thus, V_{bi} is 0.2 V in this device structure.

The hole mobilities from PRPD3T:PCBM, PRPDBDT-O:PCBM, PRPDBDT-T:PCBM and PRPDDPP:PCBM blend films were 2.13×10^{-7}, 3.27×10^{-7}, 1.40×10^{-6} and 5.20×10^{-6} $cm^2V^{-1}s^{-1}$, respectively. This increasing tendency from PRPD3T to PRPDDPP corresponds to the tendency of J_{SC} and FF of the polymers. Hole mobility have a great impact on charge transport. Because it is lower than electron mobility, this difference makes accumulation of electron, resulting in increasing the probability of bimolecular recombination.[39, 40] Therefore, high hole mobility decreases the difference between electron and hole mobility, which balances charge carrier mobility. This enhances the charge transport ability of polymer in PSCs by diminishing the probability of bimolecular recombination.

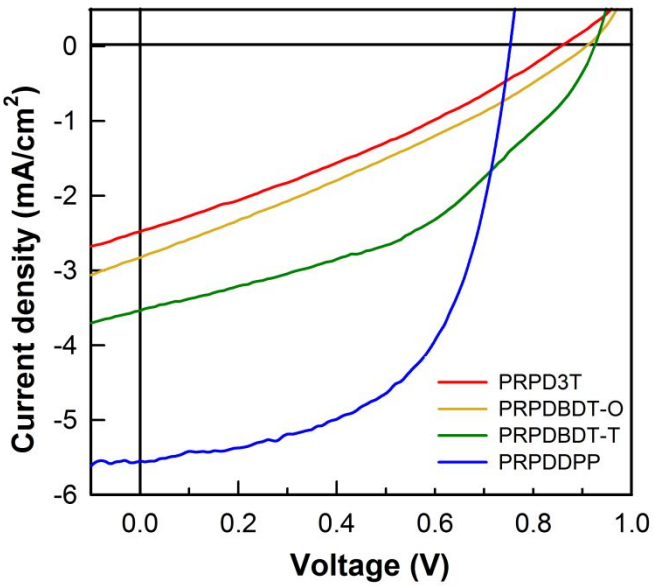

Figure 3.18 Current-voltage (*J-V*) characteristics of polymer:$PC_{71}BM$ BHJ solar cells under AM 1.5 condition

Table 3.2 Photovoltaic performances of polymers with $PC_{71}BM$ tested under standard AM 1.5G condition

Polymer	Solvent	Blend ratio (w/w)	V_{OC} (V)	J_{SC} ($mAcm^{-2}$)	FF	PCE (%)	Hole mobility[a] ($cm^2V^{-1}s^{-1}$)
PRPD3T	DCB+DIO 3vol%	1:2	0.86	2.48	0.30	0.64	2.13×10^{-7}
PRPDBDT-O	CB+DIO 0.5vol%	1:2	0.91	2.82	0.29	0.75	3.27×10^{-7}
PRPDBDT-T	CB	1:2	0.92	3.55	0.43	1.39	1.40×10^{-6}
PRPDDPP	DCB+DIO 4vol%	1:2	0.75	5.55	0.58	2.40	5.20×10^{-6}

[a] is measured by space-charge limited current methods.

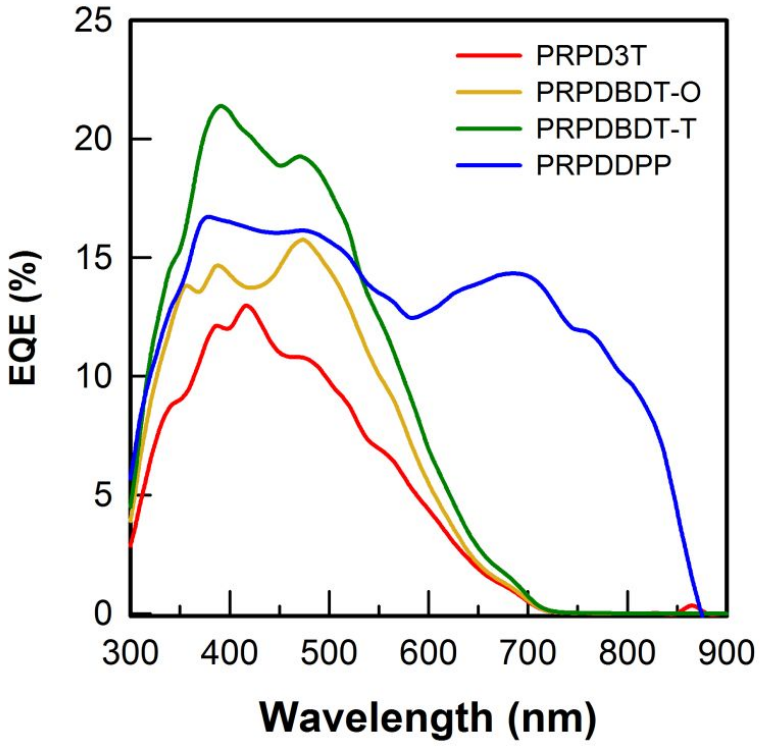

Figure 3.19 External quantum efficiency (EQE) curves of the polymer: $PC_{71}BM$ blend

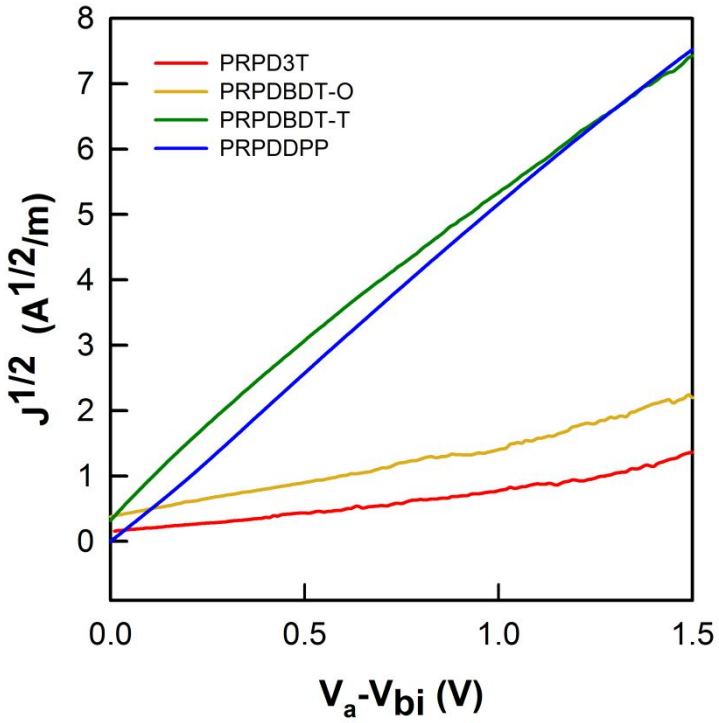

Figure 3.20 SCLC mobility of polymer:$PC_{71}BM$ blend with hole-only devices

3.7. Morphology investigation

The nanoscale internal morphologies of PRPD3T:$PC_{71}BM$, PRPDBDT-O:$PC_{71}BM$, PRPDBDT-T:$PC_{71}BM$ and PRPDDPP:$PC_{71}BM$ blend films were studied using transmission electron microscopy (TEM). The dark regions in the TEM image can be attributed to $PC_{71}BM$ domains due to its relatively high electron scattering density and the bright regions can be attributed to polymer domains. [41] In PRPD3T:$PC_{71}BM$ and PRPDBDT-O:$PC_{71}BM$ blend film, large aggregates of polymer is shown. For excitons generated in these aggregates, a distance to interface between donor and acceptor is too far to reach within exciton diffusion length. Thus, they diminish separated free charges, resulting in decrease of J_{SC}.

On the other hand, PRPDBDT-T:$PC_{71}BM$ blend film shows very smooth surface without distinct phase separation between polymer and $PC_{71}BM$. This morphology is related to structural properties of polymers. When 2-ethyl-hexylthienyl chain is attached to BDT, the intermolecular interaction is weakened due to the weakly polarized thiophene compared to oxygen and the distortion between the thiophene and BDT units. This weakens aggregation ability of PRPDBDT-T, resulted in better miscibility with $PC_{71}BM$. Good miscibility causes small domain size which is beneficial for charge separation by effective exciton diffusion to the interface between electron donor and electron acceptor. But if interconnected network is not formed, the efficiency of charge transport is decreases. Though PRPDBDT-T shows good miscibility with $PC_{71}BM$, its morphology doesn't show interconnected network structure as we can see Fig 3.21 (c). In that case, generated exciton separates into free

carges efficiently, however it is difficult that separated free charges reach to electrode. Therefore, PRPD3T, PRPDBDT-O and PRPDBDT-T needs to further morphology optimization. When chlorobenzene (CB) or o-dichlorobenzene (DCB) was used as a solvent of active layer material, PRPD3T:$PC_{71}BM$ and PRPDBDT-O:$PCB_{71}M$ show noticeable phase separation. If 1,8-diiodooctane (DIO) is added slightly as a additive, the size of aggregates diminishes. On the other hand, if DIO is added to CB solution of PRPDBDT-T:$PC_{71}BM$, it shows distinct phase separation. It is because DIO has very high boiling points (relative to CB and DCB) and offers good solubilization of $PC_{71}BM$.[42] Therefore, control of DIO ratio is important for optimization because the use of DIO cause different results depending on the miscibility. As we can see in Fig 3.21 (d), well optimized PRPDDPP:$PCB_{71}M$ blend film shows not only nanoscale phase separation but also interconnected network structure. As a result, PRPDDPP shows high FF and high J_{SC}.

Consequently, the miscibility of polymer with PCBM effects on the morphology of blend films. And the morphology again influences on the charge separation and hole mobility. Accordingly, photovoltaic performance is also determined. If further optimization is accomplished, PRPD3T, PRPDBDT-O and PRPDBDT-T, they will also exhibit enhanced photovoltaic performance.

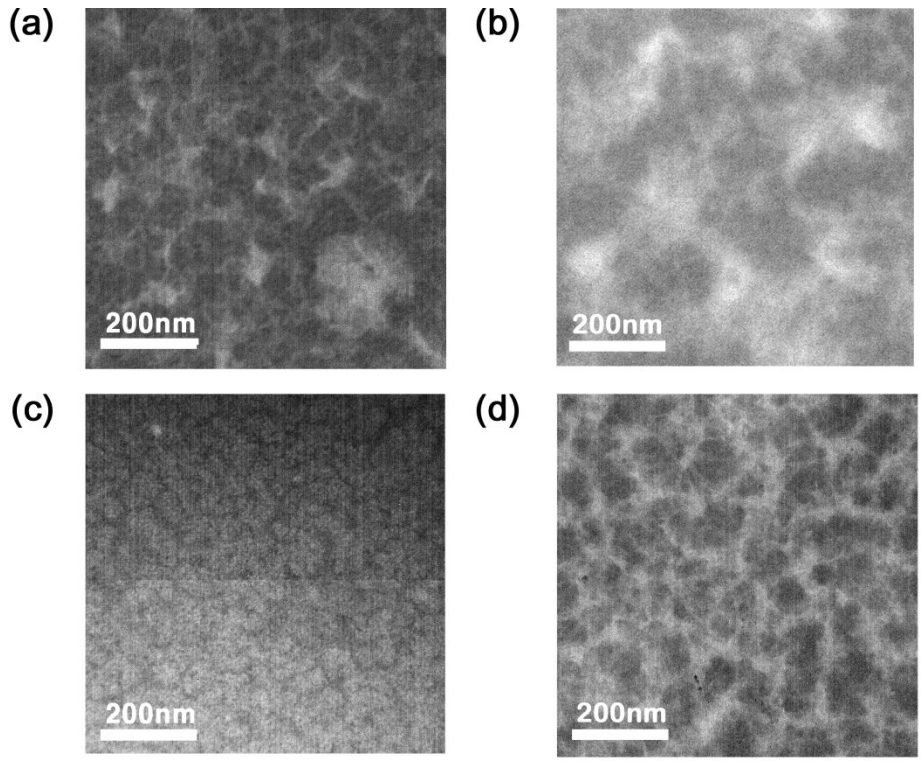

Figure 3.21 TEM images of PRPD3T:$PC_{71}BM$ (a), PRPDBDT-O:$PC_{71}BM$ (b), PRPDBDT-O/$PC_{71}BM$ (c) and PRPDDPP:$PC_{71}BM$ (d)

4. Conclusions

In this study, new electron acceptor unit, rearranged Pechmann dye was synthesized. To investigate the potential of this dye for PSCs, D-A type alternating conjugated copolymers were synthesized. RPD based alternating copolymers have wide band gap and show high V_{OC} mainly due to its low lying HOMO energy level. Among them, PRPDBDT-T and $PC_{71}BM$ blend films exhibits best PCE of 1.39% with an open-circuit voltage of 0.92 V, a short-circuit current density of 3.55 $mAcm^{-2}$, and a fill factor of 0.43 under AM 1.5G condition.

Furthermore, conjugated random copolymer PRPDDPP composed of RPD and DPP as co-electron acceptor unit was synthesized. The light absorption ranges of RPD and DPP units are completely complementary, resulting in broad absorption range from 300 nm to 900 nm. Based on broad light absorption, PRPDDPP and $PC_{71}BM$ blend films exhibits best PCE of 2.40% with an open-circuit voltage of 0.75 V, a short-circuit current density of 5.55 $mAcm^{-2}$, and a fill factor of 0.58 under AM 1.5G condition.

These results demonstrates that a new acceptor unit, RPD, is a promising building block that can be combined with many other electron donor unit, and can be utilized to supplement absorption range of low band bap polymers for high performance polymer solar cells.

Bibliography

(1) Krebs, F. C., *Polymer Photovoltaics APractical Approach*, SPIE Press, Bellingham, **2008**.

(2) Green, M. A.; Emery, K.; Hishikawa, Y.; Warta, W.; Dunlop, E. D., *Prog. Photovoltaics*, **2011**, *19*, 565.

(3) Brabec, C. J.; Sariciftci, N. S.; Hummelen, J. C., *Adv. Funct. Mater.* **2001**, *11*, 15.

(4) Coakley, K. M.; McGehee, M.D., *Chem. Mater.*, **2004**, *16*, 4533.

(5) Cheng, Y. J.; Yang, S.H.; Hsu, C.S., *Chem. Rev.*, **2009**, *109*, 5868.

(6) Hoppe, H.; Sariciftci, N. S. J., *Mater. Res.* **2004**, *19*, 1924.

(7) Thompson, B. C.; Frechet, J. M. J., *Angew. Chem., Int. Ed.* **2008**, *47*, 58.

(8) Muntwiler, M.; Yang, Q.; Tisdale, W. A.; Zhu, X. Y., *Phys. Rev. Lett.*, **2008**, *101*, 196403.

(9) Bittner, E. R.; Santos, R. J. G.; Karabunarliev, S., *J. Chem. Phys.*, **2005**, *122*, 214719.

(10) Gledhill, S. E.; Scott, B.; Gregg, B. A.; *J. Mater. Res.*, **2005**, *20*, 3167.

(11) Clarke, J. M.; Durrant, J. R., *Chem. Rev.*, **2010**, *110*, 6736.

(12) Gunes, S.; Neugebauer, H.; Sariciftci, N. S., *Chem. Rev.*, **2007**, *107*, 1324.

(13) Yu, G.; Gao, J.; Hummelen, J. C.; Wudl, F.; Heeger, A. J., *Science*, A. J., *270*, 1789.

(14) Hummelen, J. C.; Knight, B. W.; LePeq, F.; Wudl, F.; Yao, J.; Wilkins, C. L., *J. Org. Chem.*, **1995**, *60*, 532.

(15) Wienk, M. M.; Kroon, J. M.; Verhees, W. J. H.; Knol, J.; Hummelen, J. C.; van Hal, P. A.; Janssen, R. A. J., *Angew. Chem. Int. Ed.*, **2003**, *42*, 3371.

(16) Scharber, M. C.; Mühlbacher, D.; Koppe, M.; Denk, P.; Waldauf, C.; Heeger, A. J.; Brabec, C. J., *Adv. Mater*. **2006**, *18*, 789.

(17) Cheng, Y.J.; Yang, S.H.; Hsu, C.S., *Chem. Rev.*, **2009**, *109*, 5868.

(18) Ahmed, E.; Kim, F. S.; Xin, H.; Jenekhe, S. A., *Macromolecules*, **2009**, *42*, 8615.

(19) Cheng, Y.J.; Yang, S.H.; Hsu, C. S., *Chem. Rev.,***2009**, *109*, 5868

(20) Zhang, M.; Sun, Y.; Guo, X.; Cui, C.; He, Y.; Li, Y., *Macromolecules*, Y., *44*, 7625.

(21) Havinga, E.E.; Hoeve, W.T.; Wynberg, H. *Polym. Bull.* **1992**, *29*, 119.

(22) Sivula, K.; Luscombe,C.K.; Thompson, B. C.; Frechet, J.M.J., *J. Am. Chem.. Soc*., **2006**, *128*, 13988.

(23) Hou, J.; Tan, Z.; Yan, Y.; He, Y.; Yang, C.; Li, Y., *J. Am. Chem. Soc.,* **2006**, *128*, 4911.

(24) Ballantyne, A. M.; Chen, L.; Nelson, J.; Bradley, D.D.C.; Astuti, Y.; Maurano, A.; Shuttle, C. G.; Durrant, J.R.; Heeney, M.; Duffy, W.;

McCulloch, I., *Adv. Mater*. **2007**, *19*, 4544.

(25) Wu, P.T.; Xin, H.; Kim, F. S.; Ren, G.; Jenekhe, S. A., *Macromoleculs*, **2009**, *42*, 8817.

(26) Zhang, Z.G.; Wang**,** J., *J. Mater. Chem.*, **22**, *2012*, 4178.

(27) Norsten, T. B.; Kantchev, E. A. B.; Sullivan, M. B.; *Org. Lett.* **2010**, *12*, 4816.

(28) Velasco-Santos, C.; Martinez-Hernandez, A. L.; Fisher, F. T.; Ruoff , R.; Castano, V. M., *Chem Mater* **2003**, *15*, 4470.

(29) Rahmani, M.; Crombie, L., *Pertanika*, **1987**, *10*, 81.

(29) Kantchev, E. A. B.; Norsten, T. B.; Tan, M. L. Y.; Ng, J. J. Y.; Sullivan, M. B., *Chem. Eur. J.* **2012**, *18*, 695.

(30) Hou, J.; Park, M. H.; Zhang, S.; Yao, Y.; Chen, L.M.; Li, J. H.; Yang, Y., *Macromolecules*, **2008**, *41*, 6012.

(31) Jung, J.W.; Liu, F.; Russell, T.P.; Jo, W.H., *Energy Environ. Sci.*, **2013**, *6*, 3301.

(32) Lin, H.W.; Lee, W.Y., Chen, W. C., *J. Mater. Chem.*, **2012**, *22*, 2120.

(33) Hou, L.; Hou, J., *Polym. Chem.*, **2011**, *2*, 2453.

(34) Duan, R.; Ye L.; Guo, X.; Huang, Y.; Wang, P.; Zhang, S.; Zhang, J.; Huo, L.; Hou, J., *Macromolecules*, **2012**, *45*, 3032.

(35) Uhrich, C.; Schueppel, R.; Petrich, A.; Pfeiffer, M.; Leo, K.; Brier, E.; Kilickiran, P.; Baeuerle, P., *Adv. Funct. Mater.,* **2007**, *17*, 2991.

(36) Yuan, M.C.; Chiu, M.Y.; Liu, S.P.; Chen, C.M.; Wei, K.H., *Macromolecules*, **2010**, *43*, 6936.

(37) Huang, J.; Zhao, Y.; He W.; Jia, H.; Lu, Z.; Jiang, B.; Zhan, C.; Pei, Q.; Liu, Y.; Yao, J., *Polym. Chem.*, **2012**, *3*, 2832.

(38) Huang, J.; Zhan, X. C.; Zhao, Y,; Sun, Y.; Pei, Q.; Liuc, Y.; Yao, J., *Polym. Chem.*, **2013**, *4*, 2174.

(39) Moliton, A.; Nunzi, J.M., *Polym. Int.* **2006**, *55*, 583.

(40) Sun, Y.; Welch, G. C.; Leong, W. L.; Takacs, C. J.; Bazan, G. C.; Heeger, A. J., *Nature. Mater.*, **2012**, *11*, 44.

(41) Moon, J.S.; Lee, J.K.; Cho, S.; Byun, J.; Heeger, A.J.; *Nano Letters*, **2009**, *9*, 230.

(42) Dang, M. T.; Hirsch, L.; Wantz, G.; Wuest, J.D, Huang J.D., *Chem. Rev.,* **2013**, *113*, 3734.

초 록

본 연구에서는 재배열된 페크만 염료를 합성하여 고분자 태양전지의 활성층에 사용되는 전자 주개–전자 받개 형태의 고분자의 구성 요소 중 전자 받개 단위로의 활용 가능성을 확인하였다. 재배열된 페크만 염료는 전자 주개 단위로 thiophene, alkoxy-BDT, alkylthienyl-BDT를 활용하여 Stille coupling을 통해 고분자로 합성되었고, 합성된 고분자는 2.21 eV에서 2.29 eV에 이르는 넓은 밴드갭을 갖고 있었다. 이를 바탕으로 태양 전지를 제작하였을 시 0.9 V의 높은 개방전압을 나타냈고 최고 1.39%의 효율을 보였다. 나아가, 광흡수 특성을 향상시키기 위해 디케토피롤로피롤과 재배열된 페크만 연료를 전자 받개 단위로 동시에 활용하는 전도성 랜덤 고분자를 디자인하고 합성하였다. 이 고분자는 낮은 밴드갭을 갖는 동시에 넓은 영역대의 광흡수 영역을 가지고 있었고 태양전지에 적용한 결과 300 nm에서 900 nm에 이르는 넓은 빛에서 전자를 만들어내어 2.40%의 효율을 보였다. 이처럼, 재배열된 페크만 염료는 다양한 전자 주개 단위와 조합될 수 있고 낮은 밴드갭 물질의 광 흡수 영역을 보완할 수 있어 고분자 태양전지의 활성층 재료로서 높은 가능성을 보였다.

주요어: 재배열된 페크만 염료, 고분자 태양 전지, 넓은 밴드갭 공중합체, 랜덤 공중합체
학 번: 2012-20605